Available online at www.sciencedirect.com
SCIENCE DIRECT
Journal of Photochemistry and Photobiology A: Chemistry 180 (2006) 118–129
Journal of Photochemistry and Photobiology A:Chemistry
www.elsevier.com/locate/jphotochem

Fluorescence monitoring of photoinitiated polymerization reactions Synthesis, photochemical study and behaviour as fluorescent probes of new derivatives of 4′-dimethylaminostyryldiazines

P. Bosch *, C. Peinado, V. Martín, F. Catalina, T. Corrales

Instituto de Ciencia y Tecnología de Polímeros, CSIC, Juan de la Cierva 3, 28006 Madrid, Spain

Received 10 May 2005; received in revised form 6 October 2005; accepted 6 October 2005
Available online 17 November 2005

Abstract

The fluorescence emission of three new fluorescent probes has been studied in environments of different polarity and viscosity. The diazine moieties behave as electron acceptor and a good correlation has been found between their reduction potentials and the dipole moments in the excited state (estimated from solvatochromic plots using Lippert equations). The probes have shown to be sensitive to changes in both microviscosity and micropolarity of the surroundings. They have been used as fluorescent sensors to monitor the photopolymerization reactions of some mono- and difunctional methacrylate monomers in bulk. The fluorescence emission band of the probes showed an increase in intensity, as well as an hypsochromic shift, as the degree of conversion increases, throughout the entire polymerization range in the different systems checked.

Keywords: Fluorescent probes; Photopolymerization; Cure monitoring

1. Introduction

Monitoring the molecular environment of a small molecule by means of its fluorescence has been widely employed in chemistry. Such small molecules are usually designed to examine specific properties of their immediate environment or microenvironment by means of a shift in the maximum of their emission or changes in their emission intensity, and are referred to as fluorescent probes. Fluorescent molecular probes have been widely studied to measure solvent polarity and viscosity [1,2], which have been used in biochemical applications [3] and in materials science [4]. Recently, there are increasing literature reports describing fluorescent probes for testing processes occurring during polymerization. Probe fluorescence changes accompanying polymerization are related to both changes in the microviscosity and the local polarity of the medium surrounding the probe, induced by both the growth of polymer chains and the resulting polymeric solutions. Different types of fluorescent probes have been developed in recent years for monitoring photoinitiated polymerization processes: excimer forming probes [5], charge transfer (CT) probes [6] and organic salts [7]. This method offers some advantages compared to others, such as DSC and FTIR, due to its high sensitivity, selectivity and it is non-invasive. Moreover, monitoring of UV-curing processes may be committed on line which is relevant from an applied point of view.

In this work, it is described the synthesis and the photophysical study of three new probes containing an heterocyclic ring in their structures, *N*,*N*-dimethyl-[4-(2-pyridazin-3-yl-vinyl)-phenyl]-amine (DMA-2,3), *N*,*N*-dimethyl-[4-(2-pyrimidin-4-yl-vinyl)-phenyl]-amine (DMA-2,4) and *N*,*N*-dimethyl-[4-(2-pyrazin-2-yl-vinyl)-phenyl]-amine (DMA-2,5). Also, monitoring the photoinduced polymerization reactions of some mono- and difunctional methacrylate monomers in bulk has been undertaken by means of the fluorescent probes. The structures together with the abbreviations are shown in Scheme 1.

2. Experimental

2.1. Materials

Solvents (cyclohexane, *n*-hexane, carbon tetrachloride, toluene, diethyl ether, dioxane, tetrahydrofuran, ethyl acetate, chloroform, acetone, ethanol and methanol) were of analytical

* Corresponding author.
E-mail address: pbosch@ictp.csic.es (P. Bosch).

1010-6030/$ – see front matter © 2005 Elsevier B.V. All rights reserved.
doi:10.1016/j.jphotochem.2005.10.002

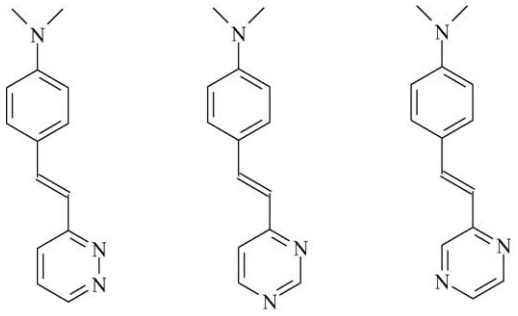

Scheme 1. Structures of the fluorescent probes together with the names used in this paper. The numbers in the names refer to the position of nitrogen atoms in the heterocyclic moiety.

grade for synthesis and spectroscopic grade for solvatochromic study. Monomers (cyclohexyl methacrylate (CHMA), lauryl methacrylate (LMA), ethylhexyl methacrylate (EHMA), hexanediol dimethacrylate (HDDMA) and diethylenglycol dimethacrylate (DEGDMA)) were purchased from Aldrich and were purified by distillation prior to use.

Chemicals (4-dimethylaminobenzaldehyde, 3-methylpyridazine, 4-methylpyrimidine, 2-methylpyrazine, sodium methoxide, *n*-butyl lithium and diisopropylamine), all of them analytical grade, were also purchased from Aldrich and used as received.

Photoinitiator bis-(2,4,6-trimethylbenzoyl)-phenylphosphine oxide (trademark Irg 819®) was generously gifted by Ciba SC and used as received.

2.2. Synthesis

N,*N*-dimethyl-[4-(2-pyridazin-3-yl-vinyl)-phenyl]-amine (DMA-2,3): 10.6 mmol of 4-methylpyridazine was added dropwise to a stirred solution of lithium diisopropylamine (LDA) (12.7 mmol) in dry THF at −40 °C under nitrogen atmosphere. After being stirred for 50 min 10.6 mmol of *N*,*N*-dimethylaminobenzaldehyde, dissolved in 25 mL of dry THF, were dropwise added. The reaction was allowed to reach room temperature and maintained stirring for 20 h. After addition of 15 mL of a saturated solution of NH_4Cl to hydrolyze the lithium salt and extraction with AcOEt, the organic phase was left over $MgSO_4$ overnight, filtered and evaporated. A mixture of the starting aldehyde, 1-(4-dimethylamino-phenyl)-2-pyridazin-3-yl-ethanol and its dehydration product (DMA-2,3) was found, which was dissolved in 20 mL of MeOH and 5 mL of concentrated HCl and refluxed for 7 h to allow the complete dehydration of the alcohol. The reaction crude was evaporated, dissolved in water, neutralized with a saturated solution of Na_2CO_3, extracted with ethyl acetate and purified through column chromatography eluting with CH_2Cl_2:AcOEt (1:9), after which a mixture of *cis* and *trans* DMA-2,3 isomers was obtained. Solid was dissolved in 40 mL of THF with a catalytic amount of I_2 and maintained refluxing during 2 h; after the isomerization reaction 0.31 g of *trans* DMA-2,3 was obtained (purity higher than 95%). The overall yield was 13%.

^{1}H NMR (δ (ppm), $CDCl_3$, 400 MHz): 2.99 (s, 6H, N(CH_3)$_2$); 6.70 (d_{ap}, J = 9.0, 2H, H_{arom}3); 7.13 (d, J = 16.3, 1H, *H*C=CH); 7.35 (dd, J = 4.8 and 8.6, 1H, H10); 7.48 (d_{ap}, J = 9.0, 2H, H_{arom}4); 7.55 (dd, J = 1.6 and 8.6, 1H, H11); 7.57 (d, J = 16.3, 1H, HC=C*H*); 8.95 (dd, J = 1.6 and 4.8, 1H, H9).
^{13}C NMR (δ (ppm), $CDCl_3$, 400 MHz): 40.24 (N(*C*H_3)$_2$); 112.08 (C_{arom}3); 120.24 (C6); 123.30 (C11); 123.94 (C5); 126.21 (C10), 128.68 (C_{arom}4); 135.38 (C7); 148.92 (C9); 153.93 (C2); 159.05 (C8).
MS (*m*/*z*): 225 (M^+, 53), 224 ($M^+ - 1$, 100), 208 (21), 170 (20).
IR (KBr, cm^{-1}): 3036, 2920, 2814 (=C–H,=C_{arom}–H, CH_3 ν); 1630, 1604, 1580, 1554 (C=C, C_{arom}=C_{arom}, C_{arom}=N ν); 1484 (–CH_3 δas); 1436 (=C–H δip); 1412 (N=N ν); 1366, 1338 (C–N δsi and δas); 1252, 1238, 1220 (C_{arom}–N δsi and δas); 1192 (C–N ν); 1168, 1152, 1086 (C_{arom}–H δip); 1004 (=C–H δoop); 958, 856, 818 (=C_{arom}–H δoop).
Microanalysis: C = 74.73% (theor: 74.64%), H = 7.06% (theor: 6.71%), N = 18.21% (theor: 18.65%).

N,*N*-dimethyl-[4-(2-pyrimidin-4-yl-vinyl)-phenyl]-amine (DMA-2,4): was synthesized by slight modification of a reported procedure [8]. 0.17 mmol of *N*,*N*-dimethylaminobenzaldehyde and 0.11 mmol of 4-methylpyrimidine were dissolved in 35 mL of dry MeOH under argon atmosphere. 0.11 mmol of MeONa were added and the reaction mixture was maintained at room temperature for 30 min. A slight increase in temperature (45 °C) led to heavy precipitation of yellow crystals. The reaction mixture was then cooled in an ice bath, filtered and the precipitate repeatedly washed with cold methanol. The solid was purified through column chromatography eluted with hexane: AcOEt (1:1), after which 1.20 g of pure *trans* DMA-2,4 were obtained (yield: 50%).

^{1}H NMR (δ (ppm), $CDCl_3$, 400 MHz): 3.00 (s, 6H, N(CH_3)$_2$); 6.69 (d_{ap}, J = 8.8, 2H, H_{arom}3); 6.82 (d, J = 15.9, 1H, *H*C=CH); 7.22 (d, J = 5.4, 1H, H11); 7.48 (d_{ap}, J = 8.8, 2H, H_{arom}4); 7.79 (d, J = 15.8, 1H, HC=C*H*); 8.56 (d, J = 5.4, 1H, H10); 9.07 (s, 1H, H9).
^{13}C NMR (δ (ppm), $CDCl_3$, 400 MHz): 40.15 (N(*C*H_3)$_2$); 111.95 (C_{arom}3); 117.91 (C11); 120.36 (C6); 123.37 (C5); 129.22 (C_{arom}4); 137.87 (C7); 151.22 (C2); 156.77 (C10); 158.70 (C9); 163.09 (C8).
MS (*m*/*z*): 226 ($M^+ + 1$, 26), 225 (M^+, 97), 224 ($M^+ - 1$, 100), 208 (47), 181 (19).
IR (KBr, cm^{-1}): 3000–2750 (=C–H, =C_{arom}–H, CH_3 st); 1606, 1570, 1520 (C=C, C_{arom}=C_{arom}, C_{arom}=N ν); 1460 (–CH_3 δas); 1360, 1304 (C–N δsi and δas); 1122 (C–N ν); 1222, 1168, 1068 (C_{arom}–H δip); 984 (=C–H δoop); 944, 876, 828, 810 (=C_{arom}–H δoop).
Microanalysis: C = 74.53% (theor: 74.64%), H = 6.63% (theor: 6.71%), N = 18.84% (theor: 18.65%).

N,*N*-dimethyl-[4-(2-pyrazin-2-yl-vinyl)-phenyl]-amine (DMA-2,5): was synthesized according to the procedure

described to obtain DMA-2,3. In this case, time of condensation reaction was 5 h and only *trans* isomer was observed after of dehydration reaction, which was isolated through column chromatography eluted with CH_2Cl_2:AcOEt (1:1). 0.74 g of pure *trans* DMA-2,4 were obtained (yield: 31%).

^{1}H NMR (δ (ppm), $CDCl_3$, 400 MHz): 2.99 (s, 6H, N(CH_3)$_2$); 6.69 (d_{ap}, J = 8.8, 2H, H_{arom}3); 6.92 (d, J = 16.1, 1H, *H*C=CH); 7.47 (d_{ap}, J = 8.8, 2H, H_{arom}4); 7.65 (d, J = 16.1, 1H, HC=C*H*); 8.29 (d_{ap}, J = 2.6, 1H, H9); 8.45 (m, 1H, H10); 8.56 (d_{ap}, J = 1.4, 1H, H11).
^{13}C NMR (δ (ppm), $CDCl_3$, 400 MHz): 40.24 (N(*C*H_3)$_2$); 112.07 (C_{arom}3); 119.18 (C6); 124.09 (C5); 128.68 (C_{arom}4); 135.39 (C7); 141.52 (C9); 143.34 (C10); 144.11 (C11); 150.89 (C2); 152.24 (C8).
MS (*m*/*z*): 226 (M^+ + 1, 36), 225 (M^+, 100), 224 (M^+ − 1, 99), 208 (58), 181 (27), 171 (20).
IR (KBr, cm^{-1}): 3000–2750 (=C–H,=C_{arom}–H, CH_3 ν); 1600, 1518 (C=C, C_{arom}=C_{arom}, C_{arom}=N ν); 1470 (–CH_3 δas); 1438 (=C–H δip); 1358, 1302 (C–N δsi and δas); 1174 (C–N ν); 1224, 1128, 1060 (C_{arom}–N δip); 974 (=C–H δoop); 946, 870, 836, 808 (=C_{arom}–H δoop).
Microanalysis: C = 74.48% (theor: 74.64%), H = 6.69% (theor: 6.71%), N = 18.83% (theor: 18.65%).

2.3. Spectroscopic measurements

Absorption spectra were recorded with a Perkin-Elmer UV–vis Lambda 16 spectrophotometer. Fluorescence spectra were obtained on a Perkin-Elmer LS 50B spectrophotometer using 355 nm as excitation wavelength and varying the slits in order to achieve better spectra for the different probes. Fluorescence spectra were corrected with the response curve of the photomultiplier. The optical densities of all the probes were in the range 0.02–0.05 at the absorption maximum. Fluorescence quantum yields were determined by comparing [9] with the usual standard solution of quinine bisulfate in 1N sulfuric acid (0.546).

2.4. Steady state irradiation

Samples of DMA-2,4 were irradiated under nitrogen in ethyl acetate at 365 nm with a Kratos high pressure mercury lamp. Absorbance of the probes during irradiation was measured by UV spectroscopy at the maximum wavelength of the charge-transfer absorption band, in a Shimatzu UV-256 FS spectrophotometer.

2.5. Polymerization proceeding and analysis

The fluorescent probe (0.002%, w/w) and photoinitiator (1%, w/w) were dissolved in the monomer to be studied. 40 μL of this formulation were placed into an aluminium pan in the DSC sample holder and the temperature maintained at 30 °C. Samples were degassed prior irradiation and then, irradiated under nitrogen in situ with a MACAM-Flexicure portable irradiation system provided with a Sylvania 400 W Hg medium-pressure lamp and twin quartz optical fiberguides. The simultaneous measuring of the fluorescence of the probe and the heat evolved in the polymerization was performed as described previously, using a shortwave pass dichroic beamsplitter to separate irradiation and emission wavelengths [10], and recording a complete fluorescence spectrum each 14 s. This dichroic beamsplitter (Lambda) shows high transmission at long wavelengths ($\lambda > 400$ nm) and high reflectivity at shorther wavelengths ($\lambda < 400$ nm). Thus, the beamsplitter was placed at 45° respect to the plane of the cell holders in a modified head of the calorimeter. In this way, the samples (40 μL) were located in the holder of the photocalorimeter. They were then front-face irradiated through an optical fiber with polychromatic light ($\lambda < 400$ nm) provided by a 400 W Hg-lamp (Macam-Flexicure). This light also acts as an excitation source for the fluorescent probes inserted as dopants into the UV-curing formulations. The light was focused to simultaneously irradiate the sample and the reference holders of the photocalorimeter. Fluorescence is collected with a fiber collimator (Spindler and Hoyer) into an optical fiber, positioned at 90° respect to the UV-excitacion beam and emission is recorded by a Perkin-Elmer spectrofluorimeter LS-50, operated in bioluminescence mode to avoid excitation light from the apparatus. A band pass optical filter centered at 313 nm (76% of transmission and 71% at 365 nm) was used to eliminate wavelengths shorther than 405 nm which overlap with the fluorescence emission spectrum.

Incident light intensity was set constant for all runs at a value of 0.75 mcal/s for monofunctional monomers and 0.36 mcal/s for difunctional ones. A value of 13.1 kcal/mol for the heat of polymerization of the methacrylic double bond was used in calculations [11].

2.6. Dipole moment determination

The excited state singlet dipole moment has been estimated by the solvatochromic method using the equations defined by Lippert [12] (Eqs. (1) and (2)).

$$\bar{\nu}_A - \bar{\nu}_F = -\frac{(\mu_e - \mu_g)^2}{4\pi\varepsilon_0 hc\alpha^3}[f(D) - f(n^2)] + [\bar{\nu}_A^0 - \bar{\nu}_F^0] \quad (1)$$

$$\bar{\nu}_A + \bar{\nu}_F = -\frac{(\mu_e^2 - \mu_g^2)}{4\pi\varepsilon_0 hc\alpha^3}[f(D) - f(n^2)] + [\bar{\nu}_A^0 + \bar{\nu}_F^0] \quad (2)$$

where ν_A^0 and ν_F^0 are respectively the frequencies (in cm^{-1}) of absorption and emission, μ_g and μ_e are the dipole moments of ground and excited states, α the radius of Onsager cavity and ε_0 is the permitivity in vacuum. The function $[f(D) - f(n^2)]$ represents the oriented polarization, where the term $f(D)$ is the total polarization and $f(n^2)$ is the induced polarization (Eqs. (3) and (4)).

$$f(D) = \frac{2(D-1)}{2D+1} \quad (3)$$

$$f(n^2) = \frac{2(n^2-1)}{2n^2+1} \quad (4)$$

where D and n are the dielectric constant and the refraction index, respectively.

Probes geometries have been optimized using Density Functional Theory (DFT) methods. It has been used standard split-valence plus polarization functions on heavy atoms 6-31G* [13] basis set and the hybrid Becke [14] three-parameterized density functional using the Lee, Yang and Paar (LYP) functional (B3LYP) [15]. Because B3LYP DFT explicitly includes electron correlation, it allows the calculation of reliable, accurate thermodynamic data. Gaussian 98, Rev. A.7 [16] and CS Chem3D Pro [17] programs have been employed for calculation and drawing. Different conformations have been carefully checked to obtain the absolute minimum energy. Harmonic vibrational frequencies have been calculated and their positive values indicate true minima.

3. Results and discussion

3.1. Synthesis

The structures of the probes are shown in Scheme 1, together with the abbreviations used, which refer to the position of the nitrogen atoms in the heterocyclic ring.

The synthesis of the probes consists in the well known Michael addition of the methyl derivative of the corresponding heterocycle to *N*,*N*-dimethylaminobenzaldehyde, followed by dehydration of the alcohol to form the conjugated double bond.

For the pyrimidine derivative, both the Michael attack and the dehydration reaction occur in the presence of the relatively weak base sodium methoxide, and the intermediate alcohol could not be isolated. This is due to the more nucleophilic nature of the methylpyrimidine carbanion, produced by the *ortho*- and *para*-position of the nitrogen atoms in the heterocyclic ring. For the pyrazine and pyridazine derivatives, the nitrogen atoms are in *ortho*- and *meta*-positions, which lead to minor reactivity of the corresponding carbanions, and then the reaction is only produced in the presence of a stronger base (LDA) and the mixture of the dehydration product together with the intermediate alcohol is obtained.

3.2. Absorption and emission properties

A description of the absorption and emission maxima of the new probes in several solvents, together with the corresponding E_T30 and π^* solvent parameters are summarized in Table 1. For DMA-2,3 the *trans* isomer was freshly obtained to assure the photophysical behaviour corresponds not to a mixture of *cis–trans* isomers.

The electronic absorption spectra present a broad band with a maximum located in the 362–400 nm regions and a shoulder around 325 nm. The shortest wavelength band corresponds to a $\pi \rightarrow \pi^*$ transition whereas the long-wavelength band, characterized by higher molar absorption coefficients, is attributed to an intramolecular CT transition. On varying the solvent polarity, moderate shifts in the absorption maxima are observed (up to 24 nm from cyclohexane to methanol). The higher red shift of the CT absorption band in DMA-2,4 and DMA-2,5 (as compared with DMA-2,3) may be explained by the increasing electron affinity of the acceptor subunit (the corresponding diazines) in the following order:

$$\text{DMA-2,3} < \text{DMA-2,4} < \text{DMA-2,5}$$

and the corresponding lowering of the CT state energies.

The electronic emission spectra are highly solvatochromic. The spectra for DMA-2,4 are shown as an example (Fig. 1).

The fluorescence maxima are strongly red shifted on increasing solvent polarity showing a batochromic shift of ca. 112 nm from cyclohexane to methanol. Quantum yields of probes in fluid media are low (1.10^{-3} to 0.11).

It is observed as a general trend that the low emission quantum yields increase with solvent polarity, whilst protic solvents such as alcohols slightly quench the fluorescence emission [18]. The red shift of their spectral position and the increase of the Stokes shift (Table 2) and of the emission bandwidth with increasing solvent polarity point out that emission comes from a CT excited state.

In order to correlate the influence of the solvent polarity on the absorption and emission maxima, we used the polarity parameters which expressed the best local interactions between the solute and the solvent, i.e., the E_T30 and π^* values [19,20]

Table 1
Maximum absorption and emission wavelengths for the probes in several solvents, and their E_T30 and π^* values

	Solvent	DMA-2,3		DMA-2,4		DMA-2,5		E_T30 (kcal/mol)	π^*
		λ_{max} abs (nm)	λ_{max} em (nm)	λ_{max} abs (nm)	λ_{max} em (nm)	λ_{max} abs (nm)	λ_{max} em (nm)		
1	Cyclohexane	364	415	378	414, 434(s)	381	398(s), 419, 441(s)	30.9	0.00
2	Hexane	362	413	375	420	379	398(s), 416, 436(s)	31.0	−0.08
3	$CC1_4$	373	433	387	438	383	439	32.4	0.28
4	Toluene	373	433	388	453	388	451	33.9	0.54
5	Diethyl ether	364	458	383	453	379	460	34.5	0.27
6	1,4-Dioxane	370	444	385	462	384	473	36.0	0.55
7	THF	370	462	390	478	384	486	37.4	0.58
8	Ethyl acetate	367	459	384	474	382	487	38.1	0.45
9	Chloroforme	378	469	396	482	391	501	39.1	0.58
10	Acetone	370	483	388	497	383	514	42.2	0.71
11	Ethanol	378	461, 557(s)	400	521	392	493	51.9	0.54
12	Methanol	378	457	402	526	392	500	55.4	0.60

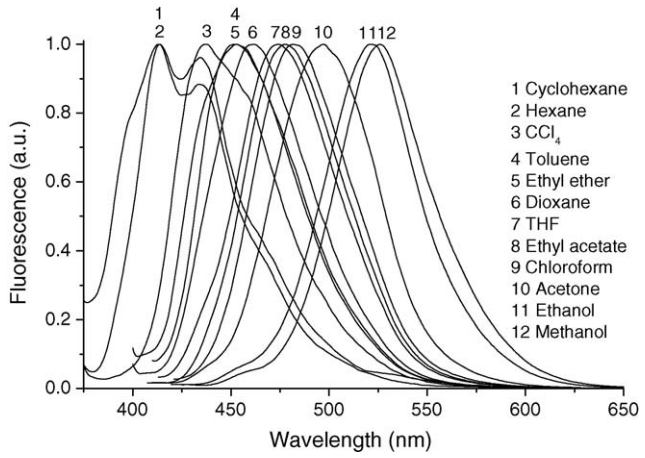

Fig. 1. Fluorescence spectra of DMA-2,4 in several solvents.

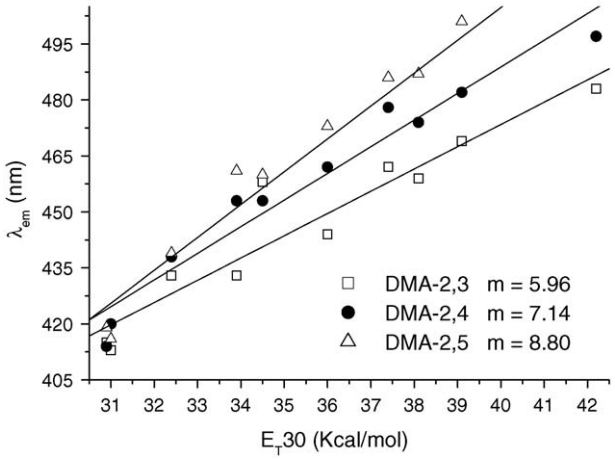

Fig. 2. Plot of the maximum emission wavelengths of probes versus E_T30 solvent parameter.

where H-bonding solvents have been excluded due to the specific solvent–solute interactions [18]. The correlations with E_T30 parameters are shown, as an example, in Fig. 2 for all probes. As can be seen, both the absorption and emission maxima correlate well with solvent polarity parameters, and the slopes of the lines are indicative of the sensitiveness towards solvent polarity. The highest solvatochromic sensitivity is observed for the styrylpyrazine (DMA-2,5) and the scattering of some data are due to specific solvent effects. For example, it is well known that dioxane is not a good solvent for solvatochromic studies.

The polarity of the solvent has a larger effect on the fluorescence spectra than on the absorption ones. Apparently, a large effective change in charge separation between the ground and the excited state is achieved. A strong donor such as dimethylamino group can produce an intramolecular charge transfer state ICT in these systems where the diazines may behave as acceptors. The two electron pairs of the diazines nitrogen atoms are in an orbital perpendicular to the aromatic π electron system, and therefore, it is difficult for these diazines to act as donors through the resonance effect. Moreover, the internal rotation of the dialkylamino group may contribute to the red-shifted fluorescence emission.

A three-state kinetic scheme is proposed to explain the photophysical behaviour of these donor–acceptor substituted stilbenes-like compounds. It is widely accepted that, in non-substituted stilbene derivatives, a double bond twisted excited isomer P^* acts as deactivation photochemical funnel, and reduces the fluorescence quantum yield of the excited E^* state. An additional third state is present if the probe has donor and acceptor subtituents. The photophysical behaviour is different from that of the stilbene and the nature of this new excited state is assigned to a ICT (intramolecular charge transfer) state, which is the responsible of the emission. Generally, in stilbene-like molecules, photoinduced internal rotations (leading for instance to twisted intramolecular charge transfer) are known to play an important role [21,22].

It is well known that the energy level of the charge transfer state is given by Eq. (5):

$$E_{CT} = E_{ox}(D) - E_{red}(A) + C \quad (5)$$

where $E_{ox}(D)$ and $E_{red}(A)$ are the electrochemical one-electron oxidation and reduction potential of the donor and acceptor groups, respectively and C is a constant that depends on the charge separation degree. As the donor group is the same dialkylamino moiety the electron withdrawing ability of each diazine may account for the differences in the emission characteristics.

Table 2
Fluorescence quantum yields and Stokes shifts of fluorescent probes in different solvents

Solvent	DMA-2,3		DMA-2,4		DMA-2,5	
	$\Phi_F \times 10^3$	$\nu_A - \nu_F$ (cm^{-1})	$\Phi_F \times 10^3$	$\nu_A - \nu_F$ (cm^{-1})	$\Phi_F \times 10^3$	$\nu_A - \nu_F$ (cm^{-1})
Cyclohexane	1	3376	2	3413	3	3571
Hexane	<1	3411	1	2857	4	3449
$CC1_4$	2	3715	2	3009	1	3331
Toluene	<1	3418	3	3698	4	4081
Diethyl ether	2	5638	3	4035	6	4646
1,4-Dioxane	2	4504	6	4329	8	4900
THF	5	5382	5	4720	9	5465
Ethyl acetate	4	5461	7	4945	10	5644
Chloroform	2	5133	4	4506	11	5615
Acetone	2	6323	12	5652	9	6654
Ethanol	3	4763	5	5806	1	5226
Methanol	<1	4573	6	5864	<1	5510

Therefore, it should be expected that not only the solvent but the nature of the acceptor chromophore has strong influence on the CT fluorescence. A good correlation between the Stokes shift in polar solvents and the reduction potential of the corresponding diazines [23] was found. This family of fluorescent sensors offers the possibility of tuning fluorescence characteristics as a function of the electron-acceptor character of the moiety which depends on the relative position of the N atoms in the diazine ring.

3.3. Dipole moments in the ground and excited state

The calculations of both geometrical parameters and the dipole moments in the ground state (Table 3 and Scheme 2) have been performed as stated in Section 2. The existence of electronic conjugation between the groups attached to the aromatic benzene ring can be seen by the length of the bonds L_1, L_2 and L_3. In the minimum energy configuration, the molecules have a planar structure in the ground state, as can be seen by the values of the dihedral angles.

The dipole moments in the singlet excited state have been estimated using the Lippert solvatochromic method, assuming that the vector of ground state is co-linear to the vector of the excited state. In Fig. 3, the plots of the Lippert solvatochromic equations for DMA-2,5 are shown as an example. If m_1 and m_2 are the slopes of both plots, and dividing Eq. (1) and Eq. (2), the following equation is obtained (Eq. (6)), which is independent of geometrical parameters and could be used to estimate the dipole moment in the excited state.

$$\frac{m_1}{m_2} = \frac{(\mu_e - \mu_g)^2}{(\mu_e^2 - \mu_g^2)} \tag{6}$$

when $m_2 > m_1$ the simplified form of this equation is given by:

$$\mu_e = \frac{m_1 + m_2}{m_2 - m_1}\mu_g \tag{7}$$

From these bases, an estimated value for the dipole moments of the singlet excited states of the probes has been obtained. It has to be pointed out that some interactions were found with specific solvents and not withstanding such ambiguity in assigning the exact dipole moment, the magnitude of μ_e implies an effective charge separation upon excitation. In Table 4, the values of the excited dipole moment of the dimethylaminos-

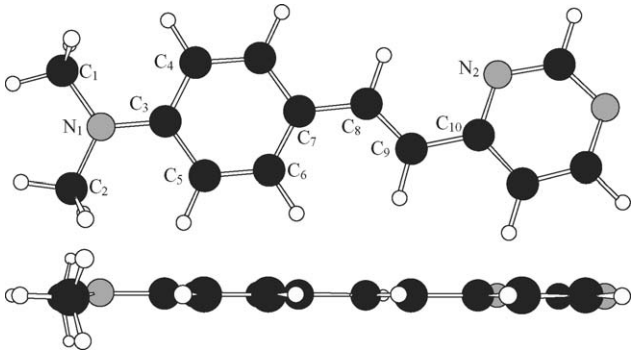

Scheme 2.

Table 3
Calculated geometrical parameters in the minimum energy configuration, and calculated dipole moments in the ground and excited states of probes

Probes	Bond lengths[a] (Å)				Dihedral angles[a] (Å)				μ_g (D)	μ_e (D)	$\Delta\mu$
	L_1, N_1–C_3	L_2, N_7–C_8	L_3, N_8–C_9	L_4, N_9–C_{10}	D_1, C_2–N_1–C_3–C_4	D_2, C_2–N_1–C_3–C_5	D_3, C_6–N_7–C_8–C_9	D_4, C_8–N_9–C_{10}–N_2			
DMA-2,3	1.383	1.455	1.352	1.461	6.544	7.329	0.420	0.054	5.4	24.9	19.5
DMA-2,4	1.381	1.453	1.353	1.458	4.719	5.058	0.206	0.012	6.6	20.7	14.1
DMA-2,5	1.383	1.455	1.352	1.458	6.500	7.067	0.499	0.054	5.0	24.7	19.7

[a] Numeration of atoms corresponds to the positions marked in Scheme 2.

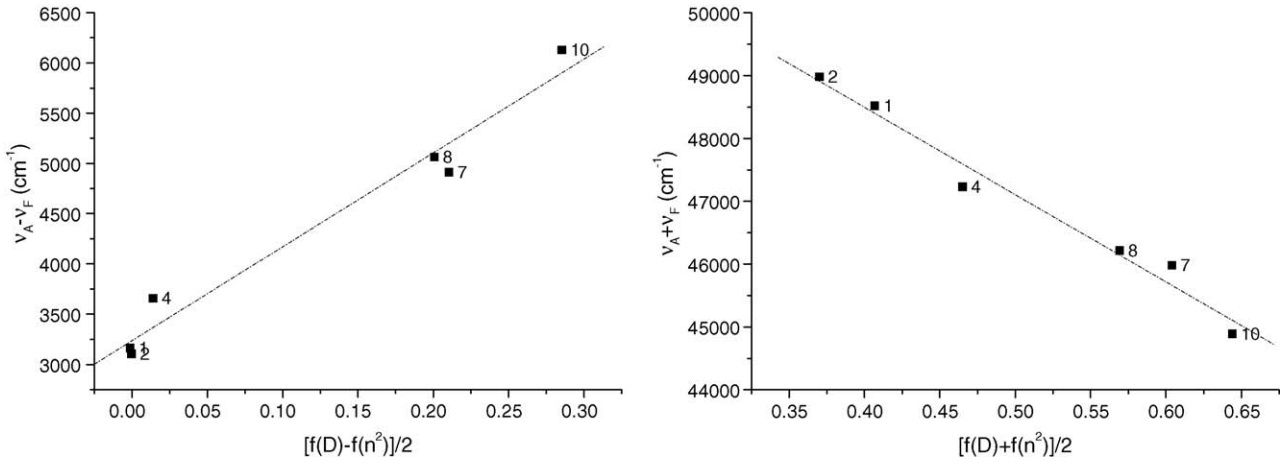

Fig. 3. Plots of the Lippert solvatochormic equations for probe DMA-2,5. (1) Cyclohexane; (2) hexane; (4) toluene; (7) THF; (8) ethyl acetate; (10) acetone.

tyryldiazines, together with the reduction potential of the corresponding electron-acceptor moiety are shown. The obtained values agree well when compared to those of other dimethylaminostyryl heterocycles [24].

3.4. Photostability

The photostability of the probes in ethyl acetate solution was checked prior to photopolymerization experiments. Negligible photobleaching was observed under direct irradiation with 365 nm light during periods of time longer than those required for complete photopolymerization (see below). However, photoisomerization of the double bond was found for DMA-2,3 up to reaching a *trans* ↔ *cis* equilibrium (80:20).

3.5. Photopolymerization in bulk of monofunctional methacrylates

For studying the suitability of the new probes for sensing photoinduced polymerization reactions, several mono- and difunctional methacrylic monomers have been chosen and photopolymerized, as described in the Section 2. Rates of polymerization and double-bond limiting conversion were measured by photo-DSC simultaneously to fluorescence variations. The kinetic behaviour of the polymerization reaction was recorded as the percentage of double bonds converted per unit of time. Equal values of rates of polymerization and limiting conversion were obtained both in the presence and absence of the probe, making then sure that the presence of the fluorophore does not affect the polymerization reaction (Fig. 4).

Kinetic profiles for photopolymerization are conventional and, except for LMA, showed an autoacceleration period. Limiting conversions for both EHMA and LMA are close to 100%, which is the normal behaviour for a monofunctional monomer. The more rigid structure of poly(cyclohexyl methacrylate) makes the reaction stops before reaching total

Table 4
Excited state dipole moment together with reduction potentials for dimethylaminostyryl heterocycles

Probe	μ_e (D)	E_{red} (eV)
4-StP-NMe$_2$[a]	14	2.15
DMA-2,4	20.7	1.78
DMA-2,3	24.9	1.61
4-StQ-NMe$_2$[a]	27	1.59
DMA-2,5	24.7	1.57

[a] From ref. [26] where 4-StP-NMe$_2$ is 4-dimethylaminostyrylpyridine and 4-StQ-NMe$_2$ is 4-dimethylaminostyrylquinoline.

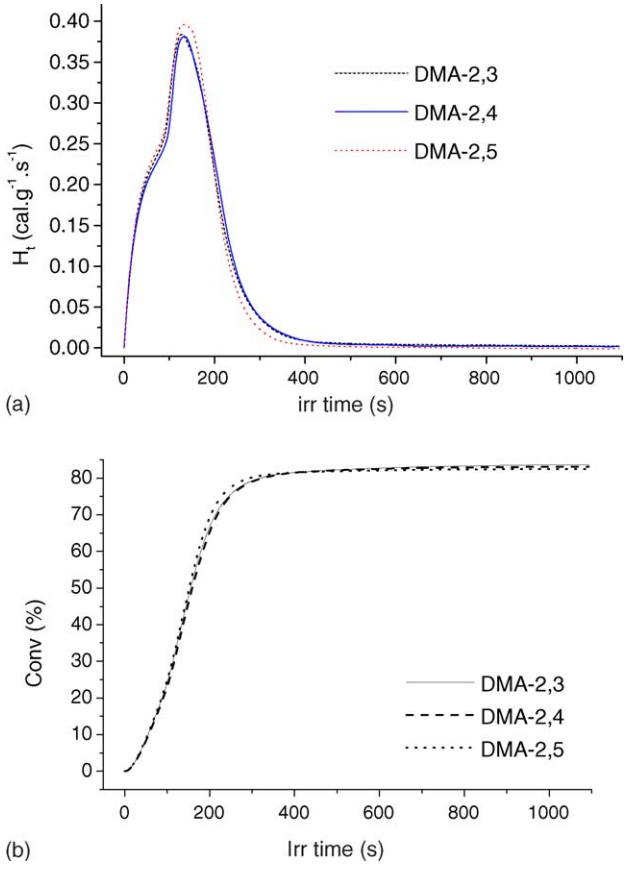

Fig. 4. Photopolymerization profile (a) and conversion–time plots (b) for cyclohexylmethacrylate photoinitiated polymerization in presence of probes.

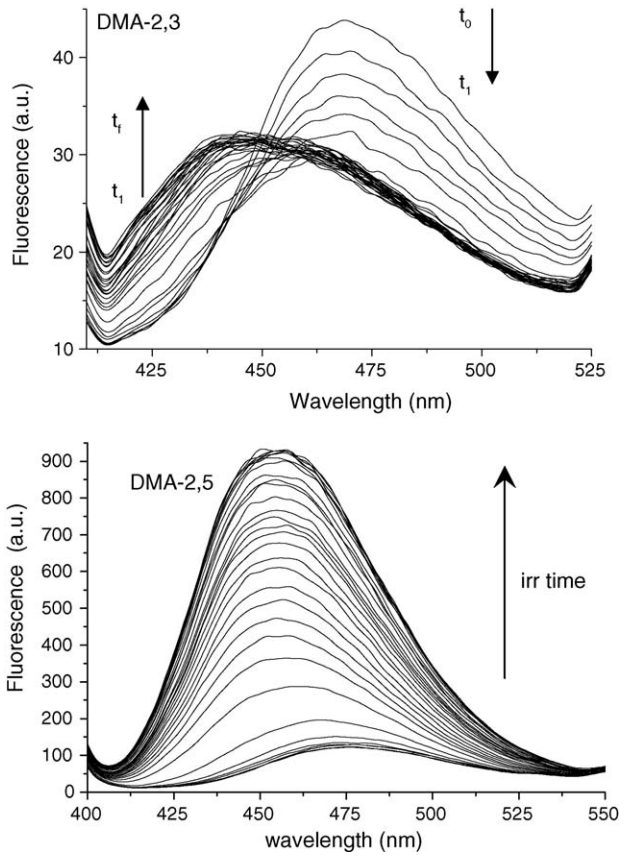

Fig. 5. Variation of fluorescence spectra of DMA-2,3 and DMA-2,5 during photopolymerization of cyclohexyl methacrylate.

conversion because T_g of *p*-CHMA is well above polymerization temperature (T_g = 377 K from ref. [11]) and vitrification of the material takes place.

The three fluorescent probes show maximum emission at wavelengths longer than 400 nm where the dicroic mirror has the transmission window which makes them suitable for our designed device. In general, fluorescence emission of probes continuously growths throughout the polymerization reactions, and an important blue shift of the band is found (Fig. 5). For a selected monomer, the blue shift of fluorescence maxima increases with the difference between the excited state and ground state dipole moment; DMA-2,4 < DMA-2,3 ~ DMA-2,5 (Table 2). The origin of emission shift towards higher energies in solvatochromic probes is related to an increasingly inefficient coupling between the excited state dipole and the microenvironment. This behaviour is typical of probes with a strong dipole moment in the excited state.

Changes in fluorescence emission band during photopolymerization have been analyzed considering three different criteria: maximum intensity, intensity ratio at two fixed wavelengths and the first moment of fluorescence, as described in detail in previous papers [25]. For all the monomers, fluorescence profiles reproduce the calorimetric plots in all the stages of the reaction. In Fig. 6, results for EHMA are shown as an example.

The kinetic parameters obtained by DSC and fluorescence for monofunctional methacrylates are summarized in Table 5. Fluorescence rates of polymerization have been calculated from the slopes of the normalized fluorescence–time plots (taking as fluorescence parameter the ratio between the intensity at two wavelengths), and the sensitivity factor, *S*, has been obtained as $S = \Delta IF/IF_0$, where ΔIF means the total increase of fluorescence emission intensity, and IF_0 is the initial fluorescence intensity.

From the experimental data some general conclusions can be draft: all probes are suitable for monitoring photopolymerization reactions of methacrylic monomers, but DMA-2,5 is the most sensitive throughout the entire range of conversion. This result agrees well with the highest solvatochromic sensitivity observed for the styrylpyrazine (DMA 2,5). It is especially remarkable that for monomers that experiment autoacceleration in their polymerization (CHMA and EHMA) this probe showed a particular increase in its fluorescence from this point (see, for instance, Fig. 6b). Before this stage of polymerization all probes showed the same behaviour. This feature can be related to a more pure ICT state of this fluorescent probe and the deactivation of non-radiative channels as result of the increasing viscosity during autoacceleration. The fluorescence band of DMA-2,3 during photopolymerization shows an isoemissive point, which seems to pinpoint the presence of different emitting states, while the shape of the fluorescence band of DMA-2,5 does not change (Fig. 5). The *trans–cis* photoisomerization may account for the presence of the isoemissive point, decreasing the intensity of the fluorescence emission at the beginning of the irradiation, up to reach *trans–cis* equilibrium. This could explain as well the lowest sensitivity of this probe.

During photopolymerization free volume fraction decreases as result of monomer conversion and a good correlation is found between the increase of fluorescence intensity ratio with conver-

Table 5
Kinetic calorimetric and fluorescence parameters for the photoinitiated polymerization of monofunctional methacrylates

Monomer	$R_p \times 10^2$ (mol/L s)[a]	Final conversion (%)	DMA-2,3			DMA-2,4			DMA-2,5		
			$\rho \times 10^2$ (mol/L s)	$\Delta\lambda$ (nm)	S[b]	$\rho \times 10^2$ (mol/L s)	$\Delta\lambda$ (nm)	S[b]	$\rho \times 10^2$ (mol/L s)	$\Delta\lambda$ (nm)	S[b]
CHMA	1.6/2.7	83	1.7, 3.3	26	0.70	0.6, 5.6	15	5.39	0.6, 6.3	22	7.25
EHMA	1.1	96	1.3	26	2.25	0.9	20	4.18	0.9	25	6.15
LMA	0.9	98	1.2	24	1.82	1.0	20	2.70	0.7	23	3.68

ρ = fluorescence rate of polymerization; $\Delta\lambda = \lambda_{init} - \lambda_{fin}$; S = sensitivity.
[a] I_0 = 0.75 mcal/s.
[b] $S = AIF_{max}/IF_0$.

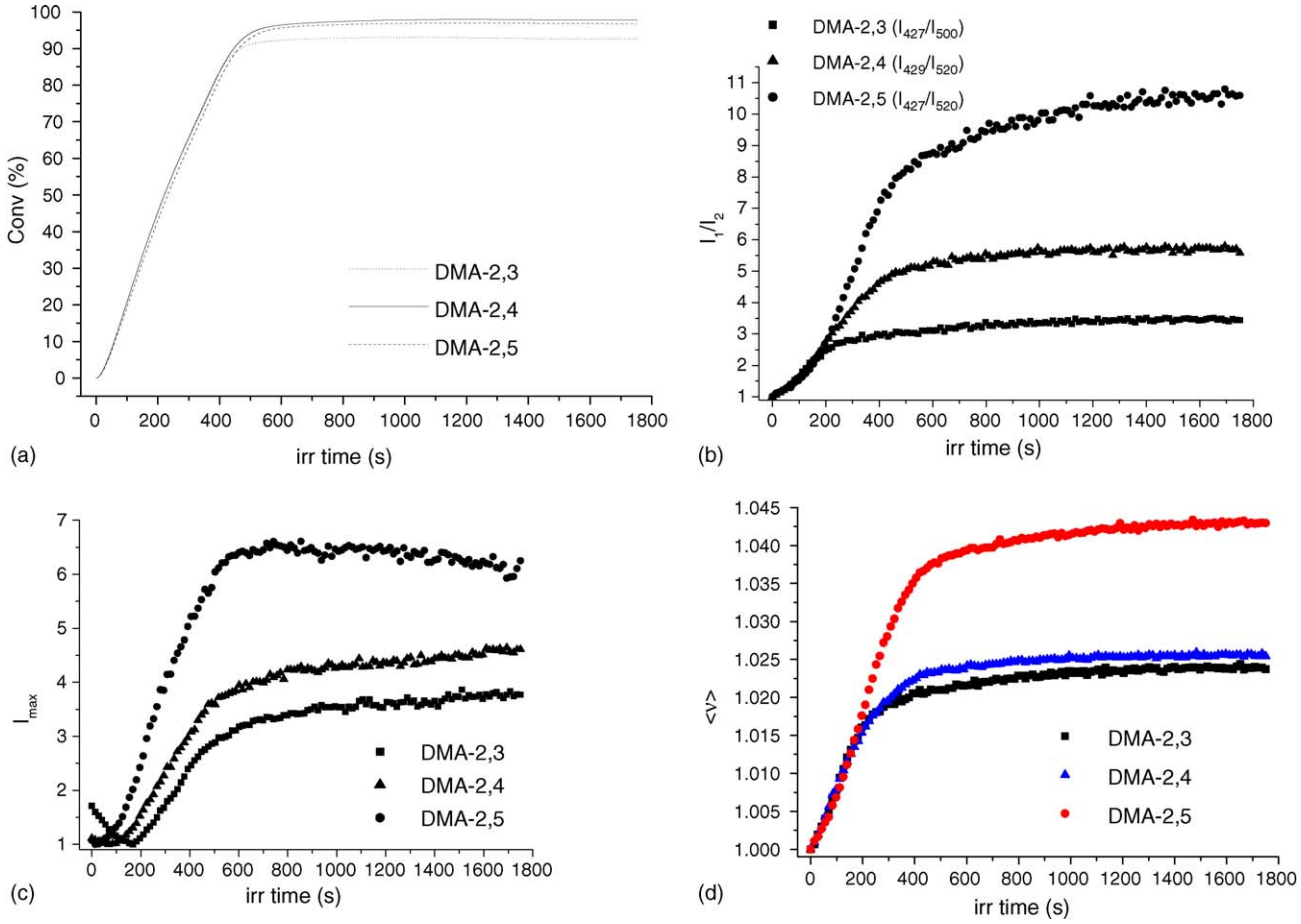

Fig. 6. Monitorization of photoinitiated polymerization of ethyl hexyl methacrylate in the presence of probes. (a) Conversion–time plot; (b) fluorescence intensity ratio–time plot; (c) maximum emission intensity–time plot; (d) first moment of fluorescence–time plot.

sion, and in the variation of the reciprocal of the free volume with conversion (Fig. 7).

This photophysical effect can be quantitatively related to changes in the non-radiative relaxation mechanism attained by the increasing rigidity of the polymer surrounding. The general expression derived by Bueche [26] in a polymer–diluent system has been used to calculate the free volume of the media:

$$V_f = 0.025 + \alpha_p(T - T_{gp})V_p + \alpha_d(T - T_{gd})V_d \quad (8)$$

where V_f is the free volume fraction, α the expansion coefficient, T_g the glass transition temperature and T is temperature. The subscrits p and d stand for the polymer and diluent, respectively. In our polymerization experiments, the monomer acts as diluent of the polymer and each read of the plot conversion time has been considered as a polymer–monomer solution. The value of α is close to $4.8 \times 10^{-4}\,^{\circ}C^{-1}$ for most polymers and $10^{-3}\,^{\circ}C^{-1}$ for most diluents. The values of T_{gd} and T_{gp} are -124 and $-10\,^{\circ}C$, respectively, for EHMA.

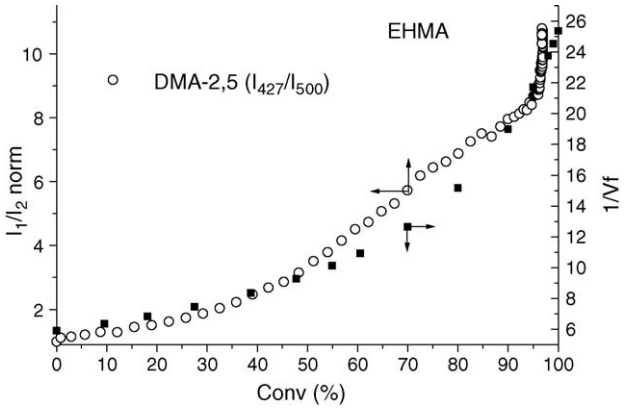

Fig. 7. Plot of the fluorescence intensity ratio of DMA-2,5 vs. conversion during the photopolymerization of EHMA. Right axis shows the reciprocal of the free volume fraction as function of the conversion.

Among the fluorescence parameters used for describing the reaction, the ratio between intensities at two wavelengths is the most adequate since it provides the highest sensitivity along the whole process and it is not necessary an internal standard for conversion determination in the different photopolymerization experiences. However, a standard curve of fluorescence against conversion should be obtained for each system monomers-probe.

Changes in fluorescence have been correlated with monomer double bond conversion (Fig. 8).

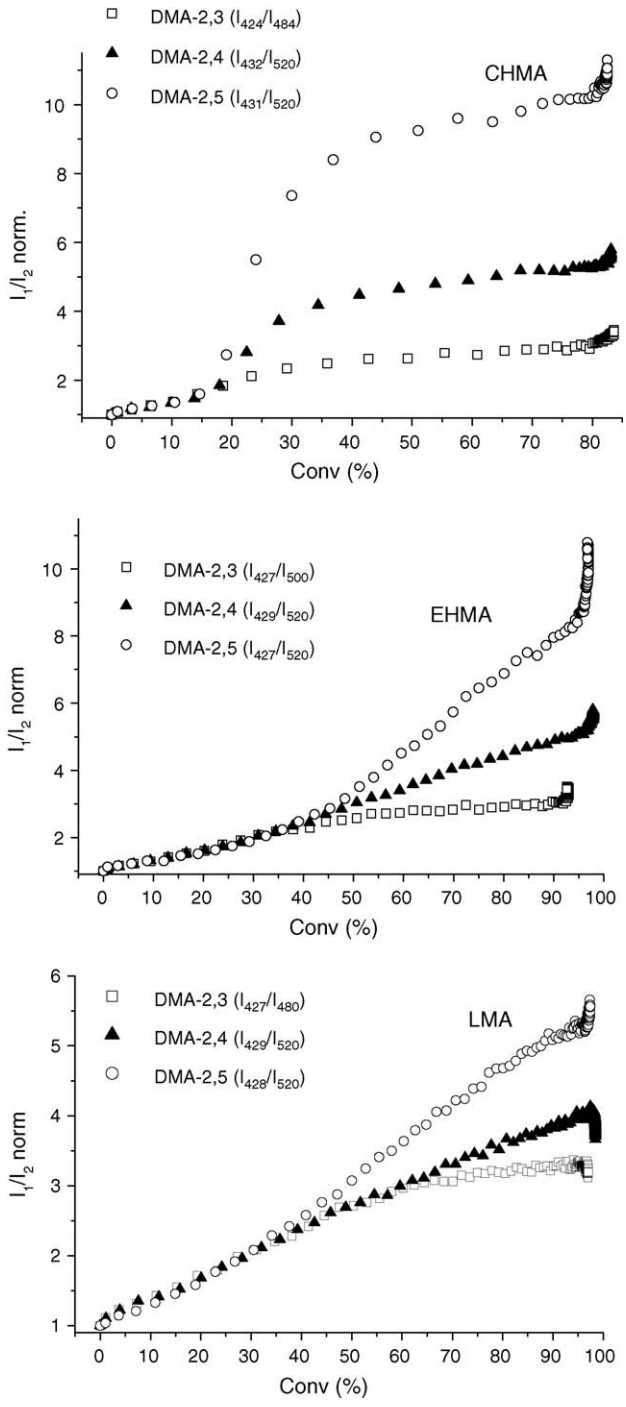

Fig. 8. Fluorescence–conversion plots for the polymerization of monofunctional methacrylates.

In these plots, the good sensitivity of the probes DMA-2,4 and DMA-2,5 until final conversion can be again observed. In addition other significant feature can be seen: the fluorescence emission from all probes (except for the LMA/DMA-2,3 and LMA/DMA-2,4 samples) continues growing at the end of the reaction after double bond conversion has reached a constant value. This is interpreted in terms of an increase in rigidification of the medium after completion of the double bond polymerization reaction, which is due to secondary crosslinking reactions. These reactions are hydrogen atom abstraction from the polymeric chains by the photogenerated initiator primary radicals. This has been observed before in the photocuring reaction of acrylic adhesives [27,28]. The decrease observed in fluorescence for the LMA/DMA-2,3 and LMA/DMA-2,4 samples is attributed to a slight photodegradation of the probes at the end of the reaction, and it is only observed at very long times for the slower LMA polymerization.

3.6. Photopolymerization in bulk of difunctional methacrylates

The photopolymerization reaction of HDDMA and DEGDMA has been performed in the same way than for monofunctional monomers and the same fluorescence and calorimetric features have been found. Kinetic data are summarized in Table 6 and fluorescence–conversion plots are shown in Fig. 9.

Rates of polymerization are higher than for monofunctional monomers, and complete polymerization takes place in less than 200 s. Limiting conversions do not exceed 60–63%, as expected for crosslinking reactions. In general, the probes behave in the same manner than for linear polymerizations, so they are also suitable for monitoring crosslinking reactions in where a high rigid medium is obtained. It is also observed the better sen-

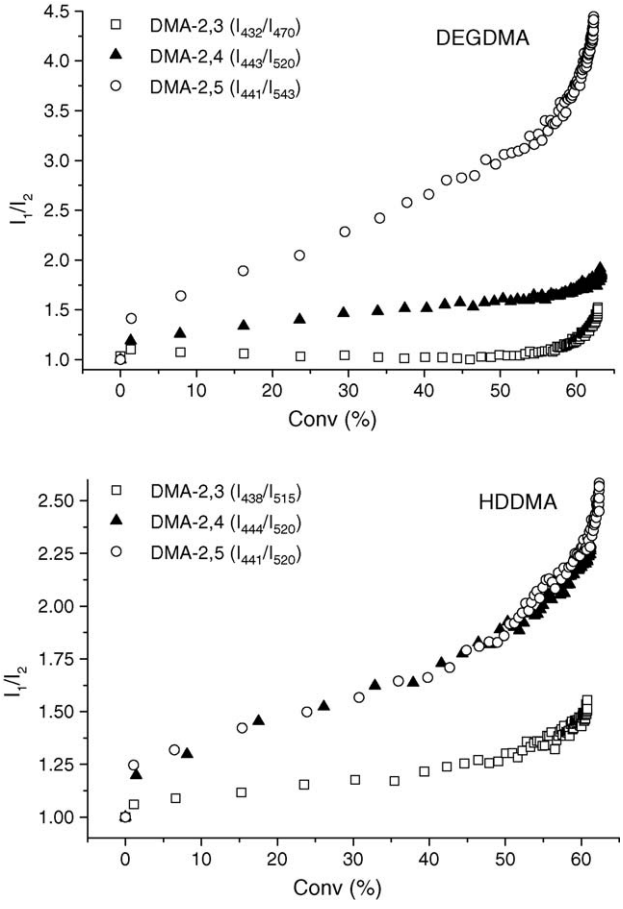

Fig. 9. Fluorescence–conversion plots for the polymerization of difunctional methacrylates.

Table 6
Kinetic calorimetric and fluorescence parameters for the photoinitiated polymerization of difunctional methacrylates

Monomer	$R_p \times 10^2$ (mol/L s)[a]	Final conversion (%)	DMA-2,3			DMA-2,4			DMA-2,5		
			$\rho \times 10^2$ (mol/L s)	$\Delta\lambda$ (nm)	S[b]	$\rho \times 10^2$ (mol/L s)	$\Delta\lambda$ (nm)	S[b]	$\rho \times 10^2$ (mol/L s)	$\Delta\lambda$ (nm)	S[b]
HDDMA	2.2	61	1.3	8	1.28	2.6	8	4.26	1.9	8	4.18
DEGDMA	2.4	63	–	–	–	2.9	6	4.12	2.2	13	5.72

ρ = fluorescence rate of polymerization; $\Delta\lambda = \lambda_{init} - \lambda_{fin}$; S = sensitivity.
[a] $I_0 = 0.36$ mcal/s.
[b] $S = AIF_{max}/IF_0$.

sitivity of DMA-2,5 and an increase in fluorescence emission of all the probes after conversion reached its limiting value. A surprising fact is that the probes seem less sensitive towards crosslinking polymerization reactions that for linear polymerization, although in the former higher rigidity is obtained. This fact could be seen in the sensitivity factor for these probes as well as the small wavelength shift of the bands, which does not exceed 13 nm for the most sensitive probe. We do not have a proper explanation for this, but new experiments are currently being performed, which will be published further.

A striking different behaviour is observed for DMA-2,3 probe monitoring fluorescence changes during photopolymerization of difunctional monomers compared to monofunctional ones. As mentioned before fluorescence emission band shows an isoemissive point during the photopolymerization of monofunctional monomers that disappears during the photopolymerization of difunctional, such as DEGDMA and HDDMA. The influence of the primary excited state on the CT emitting state may account for this behaviour in the same sense that impairs the behaviour of this probe respect to DMA-2,4 and DMA-2,5. Moreover, the *trans–cis* photoisomerization depends to a large extent on the medium, such as solvatation, temperature and, especially, viscosity. The enhacenment of viscosity has a profound effect slowing down isomerization. Therefore, the initial decrease of fluorescence emission during irradiation of monofunctional monomers it is not observed for the difunctional ones, because the increase of viscosity in this case is much higher. As photopolymerization progresses, the molecular mobility of the stilbenoid probes becomes more restricted and the photoisomerization rate diminishes [29].

4. Conclusions

Three new fluorescent probes have been synthesized and their fluorescence emission has been characterized towards changes in the polarity and viscosity of the medium.

They have been used to monitor the polymerization reaction of mono- and difunctional methacrylic monomers. As photopolymerization proceeds, the fluorescence band of the probes showed an increase in intensity as well as a spectral blue shift until final conversion. This behaviour allows following the reaction by fluorescence spectroscopy.

The fluorescent kinetic profiles accurately reproduce those obtained by photo-DSC, including the onset of the autoacceleration process. The fluorescence parameters which have been checked for following the reaction are: maximum intensity, emission ratio between intensities at two wavelengths and the first moment of fluorescence, from which emission ratio between intensities at two wavelengths has been shown to be the most adequate throughout the entire reaction.

The rate of polymerization has been measured from the fluorescence–time plots and fluorescence has been correlated with conversion measured simultaneously by differential scanning calorimetry.

All probes have been shown to be sufficiently sensitive to follow the complete polymerization reaction of mono- and difunctional methacrylic monomers, being DMA-2,5 the most sensitive among them.

It is emphasized the need of a detailed solvatochromic analysis to use fluorescent probes for monitoring polymerization.

References

[1] C. Reichardt, Chem. Rev. 94 (1994) 2319.
[2] A. Jacobson, A. Petric, D. Hogenkamp, A. Sinur, J.R. Barrio, J. Am. Chem. Soc. 118 (1996) 5572.
[3] Fluorescence spectroscopy, imaging and probes, in: R. Kraayenhof, A.J.W.G. Visser, H.C. Gerritsen (Eds.), Springer Series on Fluorescence, Berlin, Springer-Verlag, 2002.
[4] H. Itagaki, in: T. Tanaka (Ed.), Experimental Methods in Polymer Science, Academic Press, USA, 2000 (Chapter 3).
[5] (a) Ö. Peckan, Y. Yilmaz, O. Okay, Polymer 38 (1997) 1693;
(b) O. Okay, D. Kaya, O. Peckan, Polymer 40 (1999) 179.
[6] (a) J. Paczkowski, D.C. Neckers, Macromolecules 24 (1991) 3013;
(b) J. Paczkowski, D.C. Neckers, Macromolecules 25 (1992) 548;
(c) J. Paczkowski, D.C. Neckers, J. Polym. Sci. A: Chem. 31 (1993) 841;
(d) I.N. Kotchetov, D.C. Neckers, J. Imaging Sci. Technol. 37 (1993) 156;
(e) W.F. Jagger, A.A. Volkers, D.C. Neckers, Macromolecules 28 (1995) 8153;
(f) R. Popielarz, S. Hu, D.C. Neckers, J. Photochem. Photobiol. A: Chem. 110 (1997) 79;
(g) B. Strehmel, J.H. Malpert, A.M. Sarker, D.C. Neckers, Macromolecules 32 (1999) 7476;
(h) V.F. Jagger, A.M. Sarker, D.C. Neckers, Macromolecules 32 (1999) 8791.
[7] W.F. Jager, D. Kundasheva, D.C. Neckers, Macromolecules 29 (1996) 7351.
[8] D.M. Brown, G.A.R. Kon, J. Chem. Soc. (1948) 2147.
[9] D.F. Eaton, J. Photochem. Photobiol. B: Biol. 2 (1988) 523.
[10] C. Peinado, A. Alonso, E.F. Salvador, J. Baselga, F. Catalina, Polymer 43 (2002) 5355.
[11] J. Brandrup, E.H. Immergut, E.A. Grulke (Eds.), Polymer Handbook, fourth ed., John Wiley and Sons, 1999.
[12] E. Lippert, Z. Naturfosch. 10 (1995) 541.

[13] W.J. Hehre, L. Radom, P.V.R. Schleyer, J.A. Pople, Ab initio Molecular Orbital Theory, John Wiley and Sons, New York, 1986.
[14] A.D. Becke, J. Chem. Phys. 98 (1993) 5648.
[15] C. Lee, W. Yang, R.G. Parr, Phys. Rev. B B37 (1998) 785.
[16] M.J. Frisch, G.W. Trucks, H.B. Schlegel, G.E. Scuseria, M.A. Robb, J.R. Cheeseman, V.G. Zakrzewski, J.A. Montgomery Jr., R.E. Stratmann, J.C. Burant, S. Dapprich, J.M. Millam, A.D. Daniels, K.N. Kudin, M.C. Strain, O. Farkas, J. Tomasi, V. Barone, M. Cossi, R. Cammi, B. Mennucci, C. Pomelli, C. Adamo, S. Clifford, J. Ochterski, G.A. Petersson, P.Y. Ayala, Q. Cui, K. Morokuma, D.K. Malick, A.D. Rabuck, K. Raghavachari, J.B. Foresman, J. Cioslowski, J.V. Ortiz, A.G. Baboul, B.B. Stefanov, G. Liu, A. Liashenko, P. Piskorz, I. Komaromi, R. Gomperts, R.L. Martin, D.J. Fox, T. Keith, M.A. Al-Laham, C.Y. Peng, A. Nanayakkara, C. Gonzalez, M. Challacombe, P.M.W. Gill, B. Johnson, W. Chen, M.W. Wong, J.L. Andres, C. Gonzalez, M. Head-Gordon, E.S. Replogle, J.A. Pople, Gaussian 98, Revision A.7, Gaussian, Inc., Pittsburgh, PA, 1998.
[17] CS Chem3D Pro. CambridgeSoft Corporation, Cambridge, USA, 1999.
[18] P. Suppan, N. Ghoneim (Eds.), Solvatochromism, The Royal Society of Chemistry, Cambridge, UK, 1997.
[19] (a) C. Reichardt, H.F. Ebel (Eds.), Solvents and Solvent Effects in Organic Chemistry, second ed., VCH, Basel, 1998;
(a) C. Reichardt, Chem. Rev. 94 (1994) 2319.
[20] M.H. Abraham, G.J. Buist, P.L. Grellier, R.A. McGill, D.V. Prior, S. Oliver, E. Turner, J.J. Morris, P.J. Taylor, P. Nicolet, P.-C. Maria, J.-F. Gal, J.-L.M. Abboud, R.M. Doherty, M.J. Kamlet, W.J. Shuely, R.W. Taft, J. Phys. Org. Chem. 2 (1989) 540.
[21] Y. Amatatsu, Chem. Phys. 274 (2001) 87.
[22] E. Abraham, J. Oberlé, G. Jonusauskas, R. Lapouyade, C. Rulliere, J. Photochem. Photobiol. A: Chem. 105 (1997) 101.
[23] K.B. Wiberg, T.P. Lewis, J. Am. Chem. Soc. 92 (1970) 7154.
[24] S.L. Wang, T.I. Ho, J. Photochem. Photobiol. A: Chem. 135 (2000) 119.
[25] F. Mikes, F. González-Benito, B. Serrano, J. Bravo, J. Baselga, Polymer 43 (2002) 4331.
[26] F. Bueche, F.N. Nelly, J. Polym. Sci. 50 (1961) 549.
[27] C. Peinado, E.F. Salvador, J. Baselga, F. Catalina, Macromol. Chem. Phys. (20011924) 202.
[28] P. Bosch, A. Fernández-Arizpe, F. Catalina, J.L. Mateo, C. Peinado, Macromol. Chem. Phys. 203 (2002) 336.
[29] H. Meier, Angew. Chem. 31 (1992) 1399.